Diamond & Related Materials 23 (2012) 93–99

Contents lists available at SciVerse ScienceDirect

Diamond & Related Materials

journal homepage: www.elsevier.com/locate/diamond

Analytical TEM study of CVD diamond growth on TiO_2 sol–gel layers

Ying-Gang Lu [a,*], Johan Verbeeck [a], Stuart Turner [a], An Hardy [b,c], Stoffel D. Janssens [b,c], Christopher De Dobbelaere [b], Patrick Wagner [b,c], Marlies K. Van Bael [b,c], Ken Haenen [b,c], Gustaaf Van Tendeloo [a]

[a] EMAT, University of Antwerp Groenenborgerlaan 171, B-2020 Antwerp, Belgium
[b] Institute for Materials Research (IMO), Hasselt University, B-3950 Diepenbeek, Belgium
[c] IMEC vzw, IMOMEC, B-3590 Diepenbeek, Belgium

ARTICLE INFO

Article history:
Received 9 November 2011
Received in revised form 13 January 2012
Accepted 19 January 2012
Available online 26 January 2012

Keywords:
Diamond film
Plasma CVD
Diffusion
High resolution electron microscopy

ABSTRACT

The early growth stages of chemical vapor deposition (CVD) diamond on a sol–gel TiO_2 film with buried ultra dispersed diamond seeds (UDD) have been studied. In order to investigate the diamond growth mechanism and understand the role of the TiO_2 layer in the growth process, high resolution transmission electron microscopy (HRTEM), energy-filtered TEM and electron energy loss spectroscopy (EELS) techniques were applied to cross sectional diamond film samples.

We find evidence for the formation of TiC crystallites inside the TiO_2 layer at different diamond growth stages. However, there is no evidence that diamond nucleation starts from these crystallites. Carbon diffusion into the TiO_2 layer and the chemical bonding state of carbon (sp^2/sp^3) were both extensively investigated. We provide evidence that carbon diffuses through the TiO_2 layer and that the diamond seeds partially convert to amorphous carbon during growth. This carbon diffusion and diamond to amorphous carbon conversion make the seed areas below the TiO_2 layer grow and bend the TiO_2 layer upwards to form the nucleation center of the diamond film. In some of the protuberances a core of diamond seed remains, covered by amorphous carbon. It is however unlikely that the remaining seeds are still active during the growth process.

1. Introduction

The development of chemical vapor deposition (CVD) techniques has allowed the outstanding properties of diamond films to be used in a wide field of technological applications [1–5]. Previous studies have demonstrated that when titanium surfaces are modified with a TiO_2 layer, the biocompatibility and the extent of bone-implant tolerance is increased [6–8]. Combining the outstanding properties of diamond films with the excellent biocompatibility of TiO_2 layers in biomedical applications is an attractive prospect [9,10]. Most of these applications only require a very thin layer of nanocrystalline diamond and, as a consequence, the nucleation of such films need to be fully understood to guarantee thin, closed and conformal layers on 3D structures [11–14]. To realize this type of applications, diamond coatings must be produced to a high standard and with predetermined properties, which will only be possible if their nucleation and growth mechanism are thoroughly understood. Due to the high surface energy of diamond, its nucleation on non-diamond substrates is characterized by low nucleation densities and long incubation times. Consequently, surface pretreatment is commonly needed. Usually, diamond nucleation is enhanced by treating substrates by means of mechanical abrasion with diamond powder, or a mixture of diamond and other hard powders (such as Ti, Al_2O_3 etc.) [15–17], or by so-called bias enhanced nucleation (BEN) [18,19]. Mechanical treatments are simple and effective, but limited to planar surfaces, while BEN requires the substrate to be conductive. Both techniques can cause surface damage and contamination. Direct seeding with colloidal ultra dispersed diamond (UDD) is an effective solution to these problems and simultaneously enhances the diamond nucleation [20].

Besides mechanical abrasion, BEN or colloidal seeding, interlayer materials are widely used to enhance diamond nucleation and diamond film adhesion to substrates. Among others, interlayer materials like W, Ti, Zr and Ni/Cu/Ti multilayers [21,22] or intermediate layers [23] are employed to obtain adherent diamond coating on steel and WC–Co. Titanium is known to be a getter material that easily forms carbides and improves carbon adhesion to the growth interface. Carbon diffusion is also crucial for diamond nucleation and growth. The interface material plays an important role in the diffusion process of carbon. Previous studies have indicated that high quality diamond films can be grown on UDD seeds buried under a sol–gel TiO_2 layer [4]. However, mapping of the amorphous carbon distribution on diamond was not performed in these investigations.

* Corresponding author. Tel.: +32 32653331; fax: +32 3265 33 18.
E-mail address: yinggang.lu@ua.ac.be (Y.-G. Lu).

0925-9635/$ – see front matter.
doi:10.1016/j.diamond.2012.01.022

In order to further understand the influence of the TiO_2 layer on diamond film growth and gain insight into the carbon diffusion process, we investigated the early growth stages of a nanocrystalline diamond film prepared by CVD on top of sol–gel TiO_2 layers with underlying UDD seeds on a silicon substrate. The growth stages, carbon diffusion, presence of diamond and amorphous carbon, the stability of the diamond seeds and Ti diffusion phenomena are studied by analytical TEM techniques.

2. Experimental

Si substrates were cleaned with sulfuric acid/hydrogen peroxide and ammonia/hydrogen peroxide mixtures (SPM and APM, respectively), followed by an immersion for a few seconds into an aqueous colloid with nanodiamond particles of ≈10 nm in size [20]. The detonation nanodiamond powder was obtained from the NanoCarbon Institute Co., Ltd., Japan. After dispersion in water using an ultrasonic horn, no further surface treatments of the particles was done. Subsequently sol–gel nominal TiO_2 was deposited on these seeded substrates by spin-coating (3000 min^{-1}, 30 s). The precursor used was an aqueous citratoperoxo-Ti solution (pH = 7, 0.09 mol L^{-1}) synthesized as reported previously [24]. Thermal treatment was carried out on hot plates (260 °C/2 min and 450 °C/2 min). Films consisted of two layers to obtain a total thickness of approximately 10 nm. The microwave plasma enhanced (MWPE) CVD growth was carried out in an ASTeX 6500 deposition system [25]. Typical growth conditions used were as follows: H_2 and CH_4 gas flows were 485 sccm and 15 sccm, respectively. The plasma was sustained by 3500 W microwave power at a process pressure of 25 Torr, while the substrate temperature was 630 °C.

In order to investigate the different stages of early diamond film nucleation, the CVD reaction was interrupted at different growth times of 5, 10 and 20 min. A pure hydrogen plasma exposure series, using similar experimental conditions but without CH_4 was also performed in order to investigate the possible role of H_2 and its radicals on the sol–gel layer.

Cross-sectional TEM samples were prepared by focused ion beam (FIB) etching from bulk samples. In order to protect the diamond particles, a gold or chromium protection layer was deposited on top of the diamond layer prior to FIB preparation. High angle annular dark field (HAADF) images and EELS spectra were acquired using an aberration corrected FEI Titan 80–300 "cube" microscope operated in scanning transmission electron microscopy (STEM) mode equipped with a GIF Quantum spectrometer. The convergence semi-angle used was 18.5 mrad, and the acceptance angle was ~200 mrad. The microscope was operated at 120 kV in order to reduce knock-on damage by the electron beam. High resolution images and energy filtered TEM (EFTEM) images were recorded using JEOL-3000F operating at 300 kV equipped with GIF 2000 electron energy loss spectrometer [26]. The STEM-EELS spectra were quantified by multiple least squares fitting to reference spectra of the C K-edge for diamond, amorphous carbon and TiC [27].

3. Results and discussions

3.1. Nucleation and growth process

As stated above, samples were grown with CVD growth times of 5, 10 and 20 min in order to investigate the different stages of early diamond film nucleation. Fig. 1 depicts the distribution of chemical elements during the different stages of growth (oxygen map not shown). Fig. 1. (a) shows the sample after sol–gel deposition of the TiO_2 buffer layer (no plasma treatment) and Fig. 1 (b) shows a similar sample after 10 min of growth in a mixed H_2/CH_4 plasma.

The untreated sample in Fig. 1 (a) shows (from top to bottom) the amorphous carbon layer, the sol–gel TiO_2 buffer layer and some

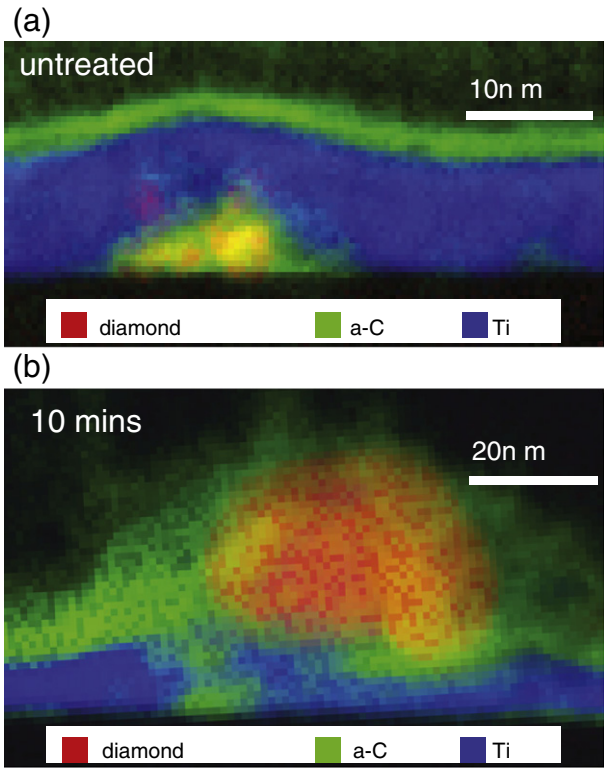

Fig. 1. Elemental maps from model-based EELS data fitting, a: untreated sample; b: 10 min $H_2 + CH_4$ treated sample.

underlying, agglomerated diamond seeds surrounded by amorphous carbon [28]. The most probable source of the continuous amorphous carbon layer on top of the TiO_2 layer are the organics remaining after the heat treatment performed on the as-deposited sol–gel precursor layer. Whether there is an influence of the amorphous carbon layer and organic residuals on the diamond nucleation process remains unclear. Fig. 2 depicts the sample after 5 min of CVD growth. The EFTEM image in Fig. 2 clearly shows that carbon clusters are formed on the surface of the TiO_2 layer. Spatially resolved scanning transmission electron microscopy (STEM)-EELS data (not shown) demonstrate these clusters indeed consist of amorphous carbon. A carbon elemental map and distribution profiles over the TiO_2 layer are also shown in Fig. 2 for this early stage of growth. Diffusion profiles (a) and (b) correspond to regions (a) and (b) indicated in the carbon map, with the diffusion direction from surface to bottom of the TiO_2 layer. The carbon signal decreases dramatically underneath the carbon clusters with increasing depth in the TiO_2 layer, but there is still a significant amount of carbon inside the titanium oxide layer. The mechanism for formation of the carbon clusters is probably related to diffusion of carbon species into the TiO_2 layer during the plasma treatment process. Carbon diffusion and saturation processes are generally believed the most crucial stages for diamond nucleation [29,30]. Some authors claim that the enhancement of diamond nucleation densities is due to the formation of carbonaceous overlayer "stocks" on top of the substrate surface under their experimental conditions [31]. In our study, we see diamond growth occurring (at later stages) only at positions on the TiO_2 layer which had diamond seeds underneath, as seen in Fig. 1 (b). From this point of view, it is unlikely that these carbon clusters act as nucleation centers for further diamond growth.

In the early stages of CVD growth, the volume of carbon underneath the TiO_2 layer increases and protuberances are formed. The increased volume arises from the conversion of UDD particles to amorphous carbon, and probably some diffusion of carbon through

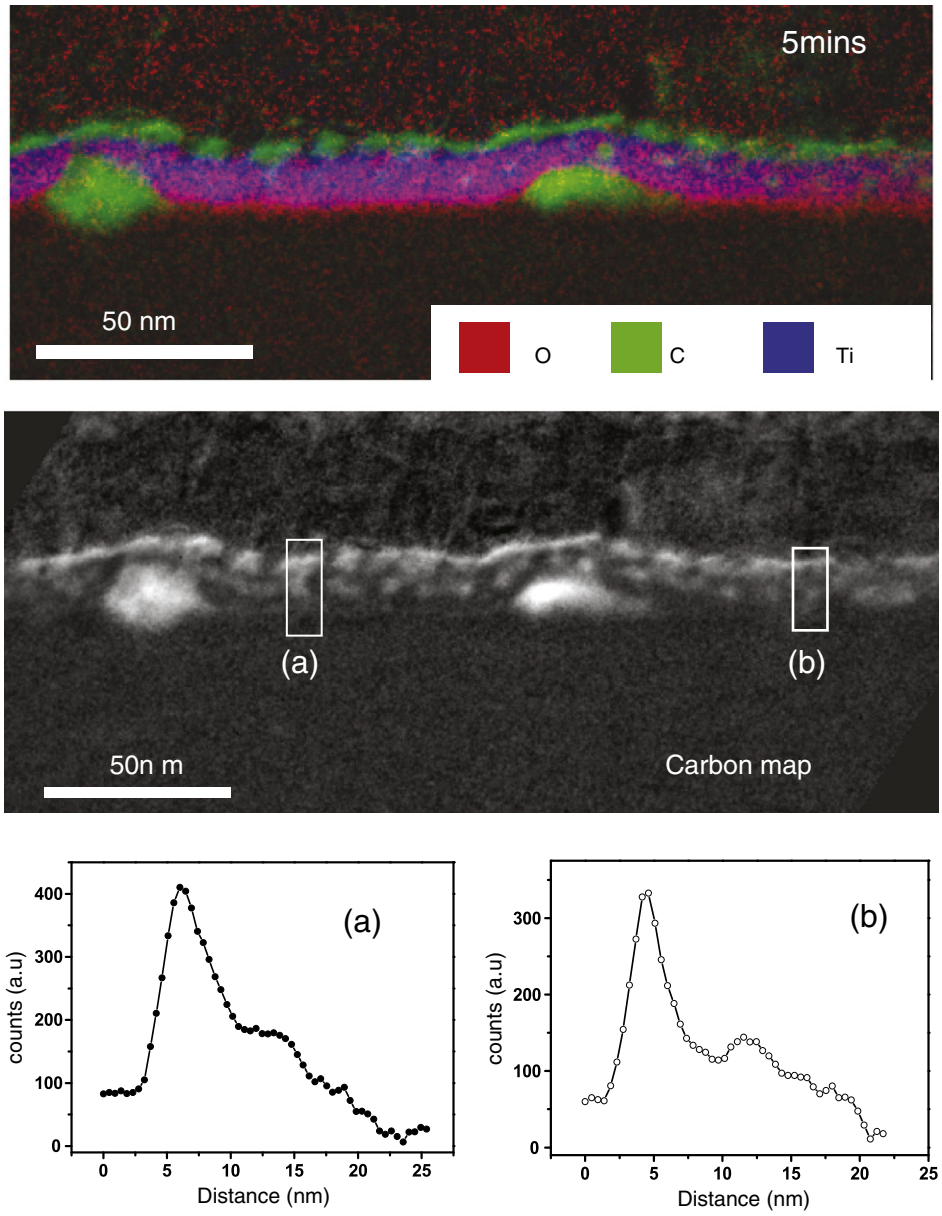

Fig. 2. EFTEM images showing carbon distribution of the 5 min H_2/CH_4 treated sample. (a) and (b) are diffusion profiles across regions a and b.

the TiO_2 layer. This effect leads to an increase in volume of the protuberances with increasing plasma exposure time. Simple volumetric calculations demonstrate that the increase in protuberance volume can largely be explained by the UDD diamond to amorphous carbon conversion.

After 10 min growth, Fig. 1 (b), bean shaped diamond particles appear on top of the titania layer surrounded by amorphous carbon clusters It should be noted that after 10 min of CVD growth, amorphous carbon is continuously distributed on and to some extent even inside the TiO_2 layer. The carbon clusters located beneath the TiO_2 layer likely originate from a diamond seed. Comparing with Fig. 1 (a), the nominal TiO_2 layer is less smooth than in the untreated sample, which indicates that the surface roughness of the TiO_2 layer changes with increasing treatment time. This is a beneficial condition for diamond nucleation. It should be noted that no TiC signal is detected between the freshly grown diamond and the TiO_2 layer, which indicates that the existence of carbide is not essential for the diamond nucleation. After 20 min, a further increase in size of the diamond particles grown on top of the layer is observed (Fig. 3). The bright-field TEM image in Fig. 3a shows an 80 nm diamond grain grown on top of a diamond seed area. The carbon map in Fig. 3b clearly shows that some carbon is still present under the titania layer, in the form of nanometer-sized seeds.

Based upon these results and further evidence from the literature [32], we present a model that explains the influence of the sol–gel TiO_2 layer on the diamond growth process; it is shown schematically in Fig. 4. Several stages in the growth process can be distinguished:

(a) During the initial stage of deposition, the buried diamond seeds are protected by the TiO_2 layer from H_2 plasma etching, but still, they transform into amorphous carbon, bulge out and lift the TiO_2 layer.
(b) Incubation stage: Hydrocarbon species arrive on the TiO_2 layer surface and are adsorbed. Adsorbed carbon species leave carbon clusters on the surface but carbon also diffuses from the top into the TiO_2 layer. UDD seeds are further converted to amorphous carbon which also diffuses into the TiO_2 layer. The incubation stage continues until the TiO_2 layer is saturated

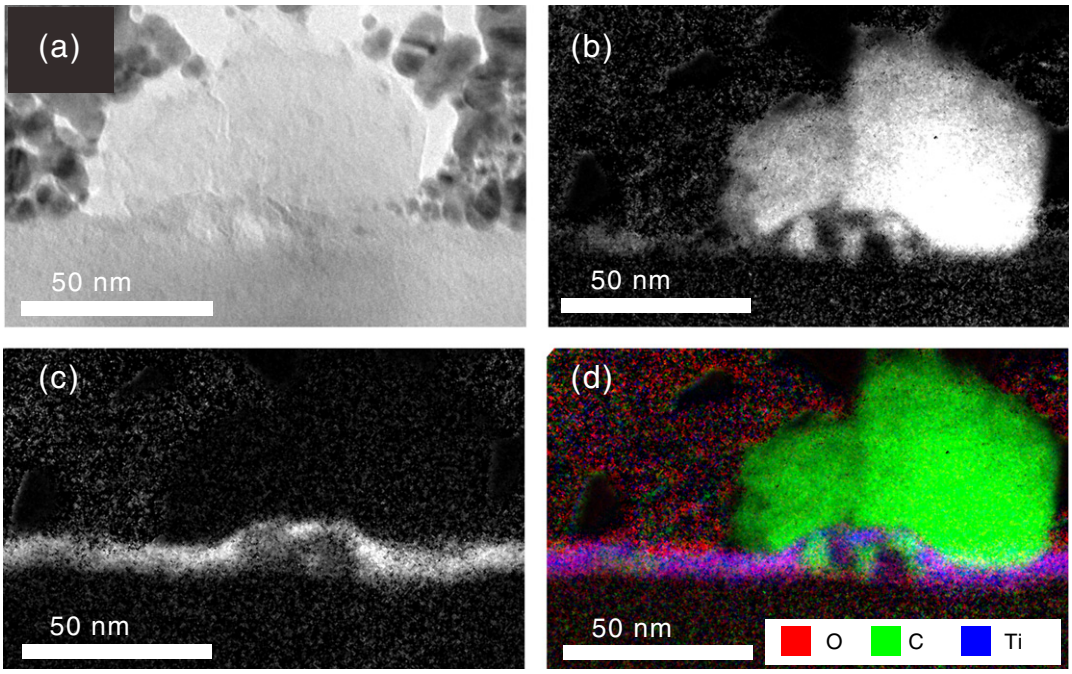

Fig. 3. 20 min growth sample; (a) bright-field TEM image; (b) carbon EFTEM map; (c) titanium map; (d) color map.

with carbon. It is reasonable to assume that thicker TiO_2 layers take longer to saturate with carbon, and will therefore display a longer incubation time.

(c) Nucleation stage: Nucleation sites are generated at the protuberances on the TiO_2 layer. As carbon diffuses from both top and bottom at these sites, carbon saturation can occur faster in these areas. At the same time, the bulged TiO_2 surface provides more roughness and enhances the field effect which can also stimulate diamond nucleation.

(d) Growth stages: After forming the nucleation center, the diamond particles continue to grow until they touch and form a continuous film.

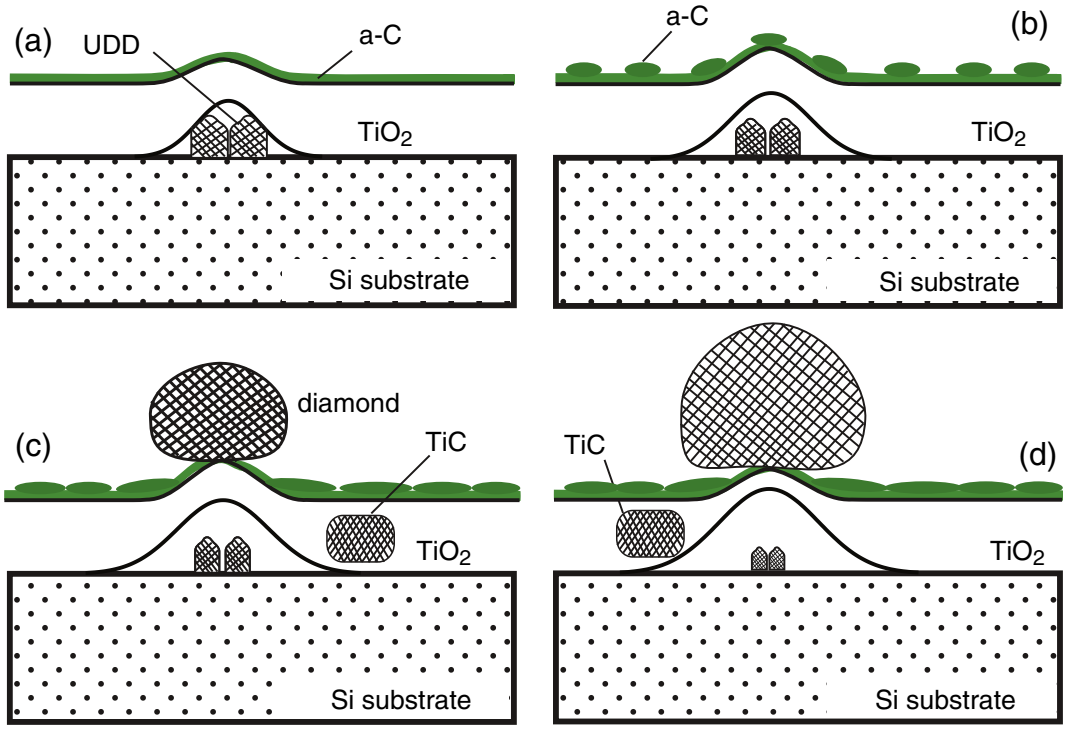

Fig. 4. Schematic showing the proposed diamond growth process on top of the TiO_2/UDD buffer layer: (a) initial stage; (b) incubation stage; (c) nucleation stage; (d) growth stage. From stage a to d, the 'bump' increases and the diamond seeds decrease in size.

3.2. The formation of TiC

There are many reports that advocate that the formation of a carbide layer is a crucial step in diamond growth [e.g. 23,33]. In order to gain insight into the possible role of TiC, HRTEM and EELS analyses were performed on the diamond film samples. HRTEM images of the 10 min sample (Fig. 5a,b) confirm the formation of nano-TiC crystallites embedded in the amorphous TiO_2 layer. This is particularly evident from the associated Fourier transforms (insets in Fig. 5a,b) where the typical diamond reflections can be identified. The amorphous region between the nano-crystallites and the substrate is probably related to partial degradation of diamond seeds due to the FIB sample preparation.

EELS data from the 20 min sample are presented in Fig. 6. The figure shows a seed region below a diamond grain that was scanned using EELS, acquiring only the carbon K-edge signal. The fine structure of the carbon K-edge is known to be a reference for its bonding state [26]. Three spectra representative of diamond, amorphous carbon and TiC are also plotted in Fig. 6. Using these references, all spectra in the scan were fitted using model-based techniques, and a diamond, amorphous carbon and TiC map were generated. As can be seen from the maps, the diamond grain was never in direct contact with the underlying diamond seed, as the titania layer is still largely intact, even after 20 min of CVD growth. A TiC interlayer is clearly located between the freshly grown diamond grain and the underlying seeds. In addition, the diamond seeds are covered by a-C, meaning they are no longer active in the diamond growth process. This also implies that homoepitaxial growth of the diamond grain on the diamond seed does not occur, contrary to other reported results [34]. Whether heteroepitaxial growth of diamond on the TiC layer/particles arises, still needs further investigation.

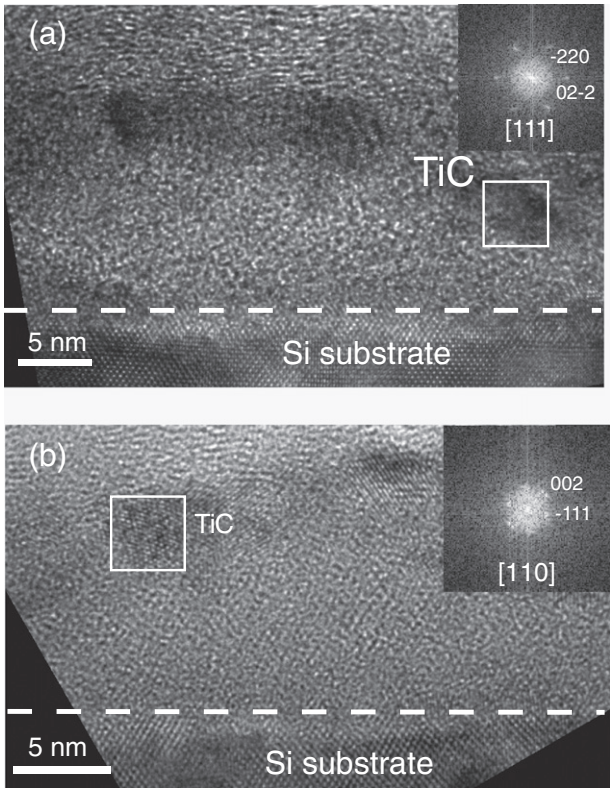

Fig. 5. (a) and (b); HRTEM images of the 10 min H_2/CH_4 treated sample. Inset Fourier transforms from square regions evidence that the crystallites are cubic TiC.

Combining the results from the 10 min and 20 min growth samples demonstrates that the formation of TiC may be an important contributing factor to diamond growth. However the results also demonstrate that the TiC formation itself is not a sufficient and necessary requirement for diamond nucleation in these samples. Pradhan et al. reported no formation of TiC under a CH_4–Ar plasma on Ti interlayer growth conditions [35]. This means that TiC formation could be strongly related to the experimental conditions. Nevertheless, this does not exclude that TiC can serve as a nucleation center. Probably, the formation of TiC plays an intermediate or secondary role in diamond nucleation and an intermediate nucleation step exists between the carbide formation and the actual diamond nucleation [33].

3.3. The stability of diamond seeds and titanium diffusion

The stability of nanodiamond seeds under plasma conditions has been studied by several groups [36–38]. Chemical interactions with reactive species and thermally activated mechanisms are all taking place simultaneously during CVD exposure. Due to the TiO_2 protection layer, the stability of the diamond seeds should be different in comparison to direct exposure to plasma. A study of the stability of diamond seeds during the early stages of growth is very important for a better understanding of the diamond nucleation mechanism.

In Fig. 7 two different diamond seed areas of a sample treated for 5 min with only H_2 (no CH_4) are displayed, together with the diamond, amorphous carbon and Ti EELS mapping results (inset to a, b). At position (a) the diamond seeds have completely converted to amorphous carbon due to the H_2 treatment. At position (b) on the other hand, a diamond seed remains, albeit covered by an amorphous carbon layer. Molecular dynamics simulations reported the etch coefficients are higher for the hydrogenated diamond (111)1*1 surface than for the hydrogenated diamond (100) 2*1 surface [39]. Even though the {111} planes are known to be predominant in nanodiamond particles, the presence of {100}-type surface truncation has also been reported [40]. The presence of a large amount of (100) truncation could explain why some diamond seeds may survive as others degrade to amorphous carbon under the same treatment condition. Another explanation for the instability of the diamond seeds is that Ti acts as a catalyst to convert the diamond seeds to amorphous carbon in the presence of atomic hydrogen [41]. From this point of view, it is clear that the diamond seeds are not active as nucleation centers, but their conversion to amorphous carbon leads to bulging of the TiO_2 film which strongly correlates to the place where diamond grains nucleate. This situation is therefore clearly different from the situation of uncovered diamond seeds [20] or seeds placed on top of a metal interlayer [17,21].

It has been demonstrated that titanium incorporated into diamond films improves the properties of diamond with respect to biocompatibility and mechanical properties [42]. However, the interface diffusion and reaction between the TiO_2 layer and the diamond film during the growth process are not fully understood to date. Fig. 8 illustrates the Ti distribution and diffusion around the grown diamond particles. The Ti has clearly diffused out of the TiO_2 layer; such diffusion profile may contain the clue as to how the diamond nucleation starts. The titanium distribution image in Fig. 8 (a) shows that the Ti has mainly diffused around the diamond nucleus. At this stage, some Ti incorporated into the diamond can not be excluded. Remarkably, no TiC signal is detected in this region.

4. Conclusions

Using a sol–gel TiO_2 layer with buried ultra dispersed diamond seeds on silicon substrates, diamond films were grown that are promising for biological applications. The early stages of this growth were

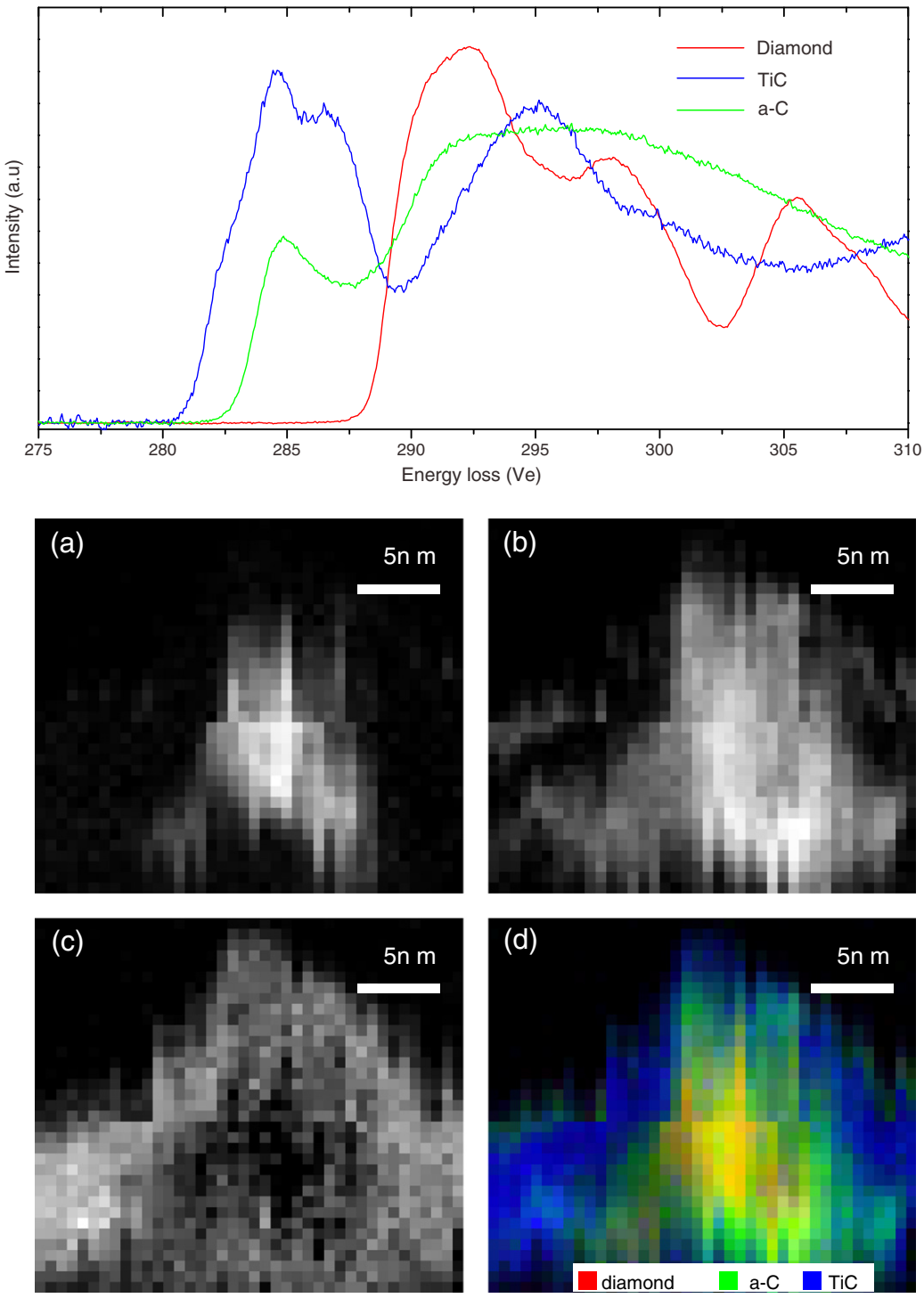

Fig. 6. Carbon K-edge fine structure EELS spectra and maps from model-based EELS data fitting of a diamond seed region under a diamond grain in the 20 min treated sample; diamond map, (b) amorphous carbon map, (c) TiC map and (d) color map.

studied in detail using advanced TEM techniques. The major conclusions are the following:

(1) EELS and EFTEM results after different growth times clearly demonstrate a carbon diffusion into the TiO_2 layer.
(2) Occasionally TiC is formed under CVD diamond growth conditions. However, there is no indication that TiC formation is a necessary condition for diamond growth.
(3) The UDD diamond seeds are not stable under CVD conditions and quickly transform into amorphous carbon. Comparing samples with and without CH_4 in the plasma seems to indicate that this amorphization is driven by the presence of H_2 and is possibly catalyzed by Ti. This increases the carbon volume and causes bulging of the TiO_2 layer. Diamond nucleation occurs exactly on top of these protuberances.

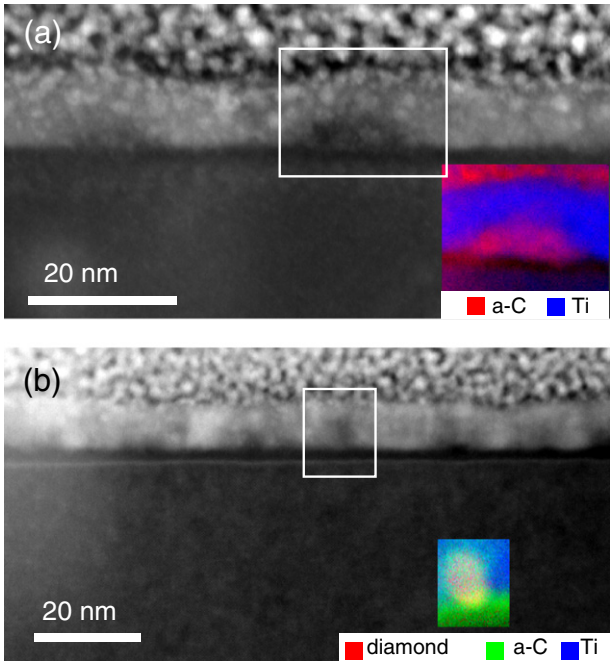

Fig. 7. (a) and (b); HAADF-STEM images of samples treated only with H_2 for 5 min, containing several UDD seeds areas. Inset; EELS model fitting results showing UDD seed elemental compositions (inset a, b). In region (a) the seeds are completely converted to amorphous carbon, in (b) the diamond seed is covered by amorphous carbon.

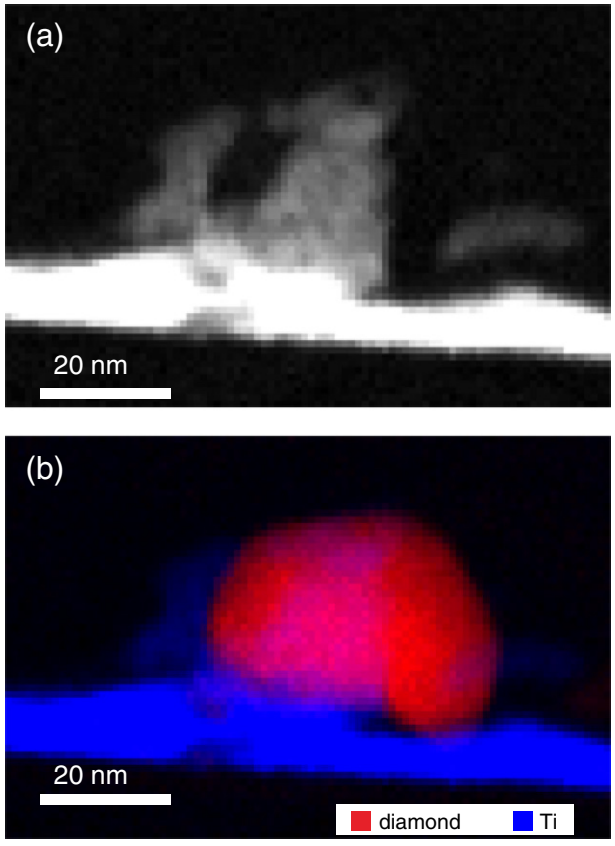

Fig. 8. (a) Ti map generated from spatially resolved EELS data. Some Ti has clearly diffused out of the TiO_2 buffer layer. (b) Color map showing the diffused Ti surrounds the diamond growth.

Acknowledgment

This work was performed within the framework of IAP P6/42 of the Belgian government. The authors acknowledge financial support from the European Union under the Framework 6 program under a contract for an Integrated Infrastructure Initiative, reference 026019 ESTEEM, from the FP7 grants DINAMO (No. 245122) and MATCON (PITN-GA-2009-238201), and FWO-G.0568.10N. Support by funding of the European Research Council under the 7th Framework Program (FP7), ERC grant No. 246791-COUNTATOMS is also acknowledged. S.T. and A.H. gratefully acknowledge the financial support from the Research Foundation-Flanders (FWO-Vlaanderen). The Titan microscope used for this work was partially funded by the Hercules Foundation.

References

[1] H. Liu, D.S. Dandy, Diamond Relat. Mater. 4 (1995) 1173–1188.
[2] F. Le Normand, J.C. Arnault, V. Parasote, L. Fayette, B. Marcus, M. Mermoux, J. Appl. Phys. 80 (1996) 1830–1845.
[3] R.S. Balmer, et al., J. Phys. Condens. Matter 21 (2009) 364221.
[4] M. Daenen, L. Zhang, R. Erni, O.A. Williams, A. Hardy, M.K. Van Bael, P. Wagner, K. Haenen, M. Nesládek, G. Van Tendeloo, Adv. Mater. 21 (2009) 670–673.
[5] J.J. Gracio, et al., J. Phys. D: Appl. Phys. 43 (2010) 374017.
[6] L. Zhu, X. Ye, G. Tang, N. Zhao, Y. Gong, Y. Zhao, J. Zhao, X. Zhang, J. Biomed. Mater. Res. Part A 78A (2006) 515–522.
[7] R. Lima, B. Marple, H. Li, K. Khor, J. Therm. Spray Technol. 15 (2006) 623–627.
[8] O. Yamamoto, K. Alvarez, Y. Kashiwaya, M. Fukuda, Carbon 49 (2011) 1588–1598.
[9] M.S. Amin, L.K. Randeniya, A. Bendavid, P.J. Martin, E.W. Preston, Diamond Relat. Mater. 18 (2009) 1139–1144.
[10] L.K. Randeniya, A. Bendavid, P.J. Martin, M.S. Amin, R. Rohanizadeh, F. Tang, J.M. Cairney, Diamond Relat. Mater. 19 (2010) 329–335.
[11] A. Krüger, Angew. Chem. Int. Ed. 45 (2006) 6426–6427.
[12] F.R. Kloss, R. Gassner, J. Preiner, A. Ebner, K. Larsson, O. Hächl, T. Tuli, M. Rasse, D. Moser, K. Laimer, E.A. Nickel, G. Laschober, R. Brunauer, G. Klima, P. Hinterdorfer, D. Steinmüller-Nethl, G. Lepperdinger, Biomaterials 29 (2008) 2433–2442.
[13] F.R. Kloss, D. Steinmüller-Nethl, R.G. Stigler, T. Ennemoser, M. Rasse, O. Hächl, Clin. Oral Impl. Res. 22 (2010) 699–705.
[14] L. Grausova, A. Kromka, Z. Burdikova, A. Eckhardt, B. Rezek, J. Vacik, K. Haenen, V. Lisa, L. Bacakova, PLoS One 6 (2011) e20943.
[15] R. Shima, Y. Chakk, A. Hoffman, Carbon 38 (2000) 1839–1843.
[16] R. Shima, Y. Chakk, M. Folman, A. Hoffman, F. Lai, S. Prawer, J. Vac. Sci. Technol. B 17 (1999) 1912–1918.
[17] J.G. Buijnsters, L. Vázquez, J.J. ter Meulen, Diamond Relat. Mater. 18 (2009) 1239–1246.
[18] M. Eckert, V. Mortet, L. Zhang, E. Neyts, J. Verbeeck, K. Haenen, A. Bogaerts, Chem. Mater. 23 (2011) 1414–1423.
[19] A. Chavanne, J.C. Arnault, J. Barjon, J. Arabski, Surf. Sci. 605 (2011) 564–569.
[20] O.A. Williams, O. Douhéret, M. Daenen, K. Haenen, E. Osawa, M. Takahashi, Chem. Phys. Lett. 445 (2007) 255–258.
[21] N.N. Naguib, J.W. Elam, J. Birrell, J. Wang, D.S. Grierson, B. Kabius, J.M. Hiller, A.V. Sumant, R.W. Carpick, O. Auciello, J.A. Carlisle, Chem. Phys. Lett. 430 (2006) 345–350.
[22] M. Daenen, O.A. Williams, J. D'Haen, K. Haenen, M. Nesládek, Phys. Status Solidi (a) 203 (2006) 3005–3010.
[23] R. Haubner, B. Lux, Int. J. Refract. Met. Hard Mater 24 (2006) 380–386.
[24] A. Hardy, J. D'Haen, M. Van Bael, J. Mullens, J. Sol-Gel Sci. Technol. 44 (2007) 65–74.
[25] S.D. Janssens, et al., New J. Phys. 13 (2011) 083008.
[26] R.F. Egerton, Electron Energy Loss Spectroscopy in the Electron Microscope, Plenum Press, New York, 1996.
[27] J. Verbeeck, S. Van Aert, Ultramicroscopy 101 (2004) 207–224.
[28] A. Krueger, M. Ozawa, G. Jarre, Y. Liang, J. Stegk, L. Lu, Phys. Status Solidi (a) 204 (2007) 2881–2887.
[29] R.H. Benno Lux, Pure Appl. Chem. 66 (1994) 6.
[30] R. Haubner, W. Kalss, Int. J. Refract. Met. Hard Mater 28 (2010) 475–483.
[31] R. Shima Edelstein, I. Gouzman, M. Folman, A. Hoffman, S. Rotter, Diamond Relat. Mater. 8 (1999) 139–145.
[32] L.-J. Chen, N.-H. Tai, C.-Y. Lee, I.N. Lin, J. Appl. Phys. 101 (2007) 064308.
[33] B.R. Stoner, G.H.M. Ma, S.D. Wolter, J.T. Glass, Phys. Rev. B 45 (1992) 11067.
[34] M. Ihara, H. Komiyama, T. Okubo, Appl. Phys. Lett. 65 (1994) 1192–1194.
[35] D. Pradhan, L.-J. Chen, Y.-C. Lee, C.-Y. Lee, N.-H. Tai, I.N. Lin, Diamond Relat. Mater. 15 (2006) 1779–1783.
[36] J.C. Arnault, S. Saada, M. Nesladek, O.A. Williams, K. Haenen, P. Bergonzo, E. Osawa, Diamond Relat. Mater. 17 (2008) 1143–1149.
[37] S. Zeppilli, J.C. Arnault, C. Gesset, P. Bergonzo, R. Polini, Diamond Relat. Mater. 19 (2010) 846–853.
[38] J.C. Arnault, S. Saada, O.A. Williams, K. Haenen, P. Bergonzo, M. Nesladek, R. Polini, E. Osawa, Phys. Status Solidi (a) 205 (2008) 2108–2113.
[39] M. Eckert, E. Neyts, A. Bogaerts, Chem. Vap. Depos. 14 (2008) 213–223.
[40] S. Turner, O.I. Lebedev, O. Shenderova, I.I. Vlasov, J. Verbeeck, G. Van Tendeloo, Adv. Funct. Mater. 19 (2009) 2116–2124.
[41] R. Shima-Edelstein, I. Gouzman, A. Hoffman, Carbon 39 (2001) 337–342.
[42] P.V. Bharathy, D. Nataraj, P.K. Chu, H. Wang, Q. Yang, M.S.R.N. Kiran, J. Silvestre-Albero, D. Mangalaraj, Appl. Surf. Sci. 257 (2010) 143–150.